Nanoscale

PAPER

View Article Online
View Journal | View Issue

Cite this: *Nanoscale*, 2016, **8**, 17340

Fluorescent polymeric nanovehicles for neural stem cell modulation†

S. A. Papadimitriou,[a] M. P. Robin,[b] D. Ceric,[c] R. K. O'Reilly,[b] S. Marino[c] and M. Resmini*[a]

Received 14th August 2016,
Accepted 20th September 2016

DOI: 10.1039/c6nr06440j

www.rsc.org/nanoscale

Nanomaterials are emerging as strong candidates for applications in drug delivery and offer an alternative platform to modulate the differentiation and activity of neural stem cells. Herein we report the synthesis and characterization of two different classes of polymeric nanoparticles: *N*-isopropylacrylamide-based thermoresponsive nanogels RM1 and P(TEGA)-*b*-P($_{D,L}$LA)$_2$ nano-micelles RM2. We covalently linked the nanoparticles with fluorescent tags and demonstrate their ability to be internalized and tracked in neural stem cells from the postnatal subventricular zone, without affecting their proliferation, multipotency and differentiation characteristics up to 150 μg ml^{-1}. The difference in chemical structure of RM1 and RM2 does not appear to impact toxicity however it influences the loading capacity. Nanogels RM1 loaded with retinoic acid improve solubility of the drug which is released at 37 °C, resulting in an increase in the number of neurons, comparable to what can be obtained with a solution of the free drug solubilised with a small percentage of DMSO.

Introduction

Ageing, neurodegenerative diseases and neurovascular disorders are increasingly common conditions associated with major irreversible loss of neurons and glial cells, resulting in high mortality and high health care costs.[1] Traditionally, neurodegenerative diseases have been clinically approached by alleviation of major symptoms. A number of promising strategies, designed to achieve brain protection, repair and recovery, have been investigated, such as delivery of neuroprotective compounds to prevent cellular degeneration,[2] use of tissue engineering, cell replacement and cell transplantation.[3] However sustained bioavailability and poor cell survival and integration in the host have considerably limited the applications.

A more recent and attractive approach has focused on targeting endogenous neural stem cells (NSC), an important reservoir of self-renewing and multipotent cells that can drive regeneration and repair, hence conferring a certain degree of plasticity to the adult brain.[2] The subventricular zone (SVZ) of the lateral ventricle and the subgranular zone of the dentate gyrus are the best characterized neurogenic areas in the adult mammalian brain.[3,4] Their identification and characterization has opened novel opportunities to design strategies aiming at replenishing depleted neurons by means of increasing the pool of endogenous progenitors, and controlling the differentiation towards a specific lineage.[5]

In recent years developments in nanotechnology, in particular with novel functional nanomaterials characterized by high surface to volume ratio, very small size and low polydispersity, have led to interesting results in the field of drug delivery, especially targeting the brain.[6] Among the different materials investigated poly(alky cyanoacrylates), such as poly(butyl cyanoacrylate) (PBCA)[7] or poly(isohexyl cyanoacrylate) (PIHCA),[8] poly(lactic acid) (PLA),[9] human serum albumin (HSA),[10] chitosan[11] and magnetic nanoparticles[12] have shown promising results.[13] These materials frequently function as excipients but are commonly described as drug delivery systems. The cargos include a variety of small molecule drugs as well as growth factors, proteins and macromolecules, well known for their pharmacological activities in the brain, like nerve growth factor (NGF),[7] doxorubicin,[8] siRNA,[14] curcumin and retinoic acid.[15] More recently the potential application of polyethyleneimine (PEI) based nanoparticles for neural drug delivery has also been reported using retinoic acid, a drug known to promote neuronal differentiation but limited by low solubility in aqueous solutions and rapid cellular metabolism.[16]

The cationic nature of PEI allows disruption of the endosomes and phagosomes created during the internalization of the nanoparticles from the cells, *via* the 'proton sponge' effect,

[a]*School of Biological and Chemical Science, Queen Mary University of London, London E1 4NS, UK. E-mail: m.resmini@qmul.ac.uk*
[b]*Department of Chemistry, University of Warwick, Coventry CV4 7AL, UK*
[c]*Blizard Institute, Barts & The London School of Medicine and Dentistry, Queen Mary University of London, E1 2AT, UK*

†Electronic supplementary information (ESI) available. See DOI: 10.1039/c6nr06440j

allowing the release of the encapsulated drug in the cytosol.[17,18] The ability of PEI to mediate endocytosis of nanoparticles was demonstrated with magnetic polymeric nanospheres,[19] using a fluorescent tag encapsulated in the polymer matrix. However the concerns and data available regarding the cytotoxicity of PEI based delivery agents, as a result of their polycationic nature represent a limitation to such systems.[20,21]

The literature available on this topic suggests that the morphology and physical chemical characteristics of the nanosystems have considerable impact on their suitability to be used for drug delivery *in vivo*. The flexibility of the matrices and their stability in aqueous environment can influence their membrane permeability and ultimately the bioavailability of the drug.

The aim of this work was to develop fluorescent polymeric nanoparticles that could act as delivery vehicle for neural stem cells, allowing tracking of cell internalization by fluorescence microscopy, and contribute to the understanding of how nanoparticle morphology can impact suitability for drug delivery applications. We synthesized and characterized two different types of polymeric nanoparticles, a thermoresponsive *N*-isopropylacrylamide (NIPAM) based crosslinked nanogel and a self-assembled block copolymer micelle system, and we covalently tagged the two nanosystems with fluorescent labels.[22,23] We demonstrate that both sets of nanoparticles are efficiently internalized in murine neural stem cells, show no evidence of toxicity and do not impact on proliferation, self-renewal and differentiation, in concentrations up to 150 μg ml^{-1}. Successful loading of retinoic acid[24,25] was achieved, although the different rigidity of the polymeric systems has a significant effect on the loading capacity of the two nanoparticles. NIPAM based nanogels were selected for *in vitro* experiments on SVZ CD 133^{+} murine neural stem cells, based on their ability to encapsulate a higher amount of pharmaceutically active ingredient. Their pharmacological activity as drug delivery systems was evaluated in comparison to the free drug in solution.

Results and discussion

Fluorescent nanoparticles

The ability to visualize nanoparticles during cellular uptake is a key priority for the development of novel delivery systems, required to validate toxicity data and confirm that the matrices are internalised. Although fluorescent labelling is one of the most common approaches for tracking nanoparticles internalization in cells, other techniques like AFM have been used lately for the same purpose.[26] Fluorescent moieties are commonly encapsulated into a polymer matrix and used for such applications, however the stability *in vitro* of these system is a cause for concern, with the tags often becoming separated from the matrix. We chose instead to covalently link the fluorophore to the backbone of the polymer structure to avoid such issues.

Given the different type of polymeric systems chosen, two fluorophores were identified. For the polymeric NIPAM nanogels, a naphthalimide-based fluorescent probe was selected, as its versatile structure allows easy chemical modification depending on the required application. The polymerizable fluorescent probe *N*-2-(6-(4-methylpiperazin-1-yl)-1,3-dioxo-1*H*-benzo[*de*]isoquinolin-2(3*H*)-yl-ethyl)acrylamide (FIM) previously reported by our group[23] was included as co-monomer in the nanogel preparation.

In the case of the block copolymer micelles, it is highly desirable to know the precise location of the fluorescent probe within the core–corona structure. This knowledge was achieved through the use of block-dye-block polymer containing the highly emissive dithiomaleimide (DTM) fluorophore, previously developed in our group, which allows precise dye incorporation at the core–corona interface of the resultant micelles.[27] This strategy has been shown to inhibit self-quenching leading to concentration-independent emission, with these particles previously demonstrated as *in vitro* contrast agents.[28] In both cases the fluorescent molecules were covalently attached to the polymer backbone, thus avoiding issues of leaking from the polymer-matrix, and generating misleading results, while the similar spectral properties of naphthalimide and DTM enabled identical imaging conditions for both systems.

One of the two systems used here is based on NIPAM nanogels. The main advantages of NIPAM-based nanoparticles are high solubility and stability, as well as ability to change the conformation, in response to variations in temperature, which allows the release of the entrapped drug. These features with their structural characteristics[29] make them strong candidates for drug delivery.

Fluorescent thermoresponsive NIPAM (RM1) based nanogels were obtained by high dilution radical polymerization, a method that allows the preparation of nanoparticles with small size (10 to 30 nm) and low polydispersity,[30] by varying the concentration of monomers and crosslinker. The best nanogel preparation was obtained by reacting 75% NIPAM, 20% methylenebisacrylamide (MBA) as crosslinker, and 5% of fluorescent probe in DMSO with a total monomer concentration (C_m) of 1%, initiated by 1% AIBN (Scheme 1). The presence of the same polymerizable unit on all reagents ensures similar reactivity rates and incorporation ratio, while the concentration of fluorescent monomer was kept low to avoid significant increase in hydrophobicity and size of the nanoparticles. The RM1 nanogels were obtained with >60% yield, were shown to have good solubility in water up to 2 mg ml^{-1} and DLS analysis of 1 mg ml^{-1} solution in water showed particle size comprised between 10–20 nm (Table 1, Fig. S1 and Table S1†), a range also confirmed by TEM, (Fig. 1A). Zeta potential was measured as −21 mV, showing that the nanogels had a slightly negative surface charge (Fig. S3†). Comparison with NIPAM nanogel particles, made in identical experimental conditions and with same percentage of crosslinker but without fluorescent co-monomer, shows similar characteristics in terms of size (Fig. S2†) and solubility, confirming the

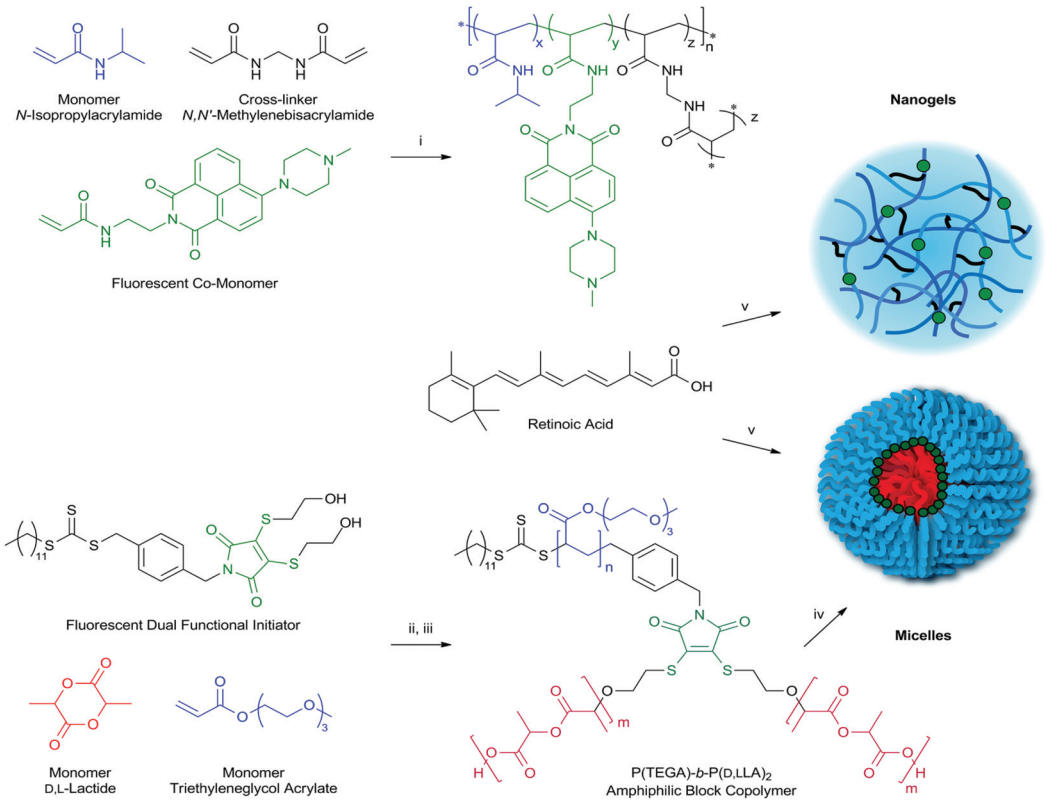

Scheme 1 Preparation of RM1 nanogels (top) and RM2 micelles (bottom), and subsequent loading with retinoic acid; (i) high dilution radical polymerization, (AIBN, DMSO, 70 °C); (ii) ring-opening polymerization of D,L-lactide (1-(3,5-bis(trifluoromethyl)phenyl)-3-cyclohexyl-thiourea, (–)-sparteine, CH_2Cl_2, room temp.); (iii) RAFT polymerization of TEGA (AIBN, $CHCl_3$, 60 °C); (iv) self-assembly *via* direct dissolution in H_2O; (v) nanoparticle loading with retinoic acid.

Table 1 Nanoparticle characterization

	$D_{h,DLS}$ (nm)	PD_{DLS}	Zeta potential (mV)	CMC[a] (g L^{-1})
RM1	9.4 ± 1.5	0.30	−21.0 ± 0.7	—
RM2	51.0 ± 0.4	0.20	−27.2 ± 2.7	0.0036

[a] Critical micelle concentration (CMC) determined by fluorescence spectroscopy.[26]

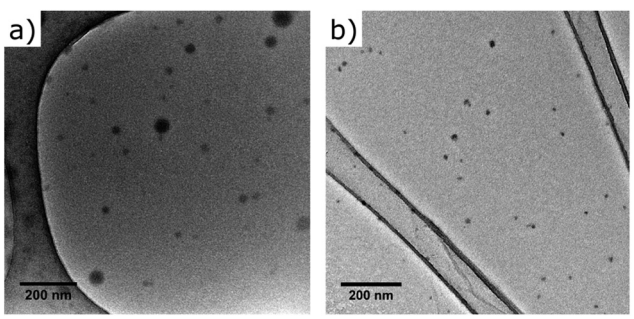

Fig. 1 Dry-state TEM images of (A) NIPAM nanogels RM1 and (B) micelles, RM2, unstained on a graphene oxide substrate.

hypothesis that the introduction of the fluorescent tag in such small quantity does not significantly impact the polymer's morphological characteristics.

DTM-labelled block copolymer micelles (RM2) were prepared according to our previously reported strategy.[27] The highly emissive DTM fluorophore was incorporated into a dual functional initiator, with subsequent ring-opening polymerization of D,L-lactide, followed by reversible addition–fragmentation chain transfer (RAFT) polymerization of triethyleneglycol acrylate (TEGA) producing an amphiphilic block copolymer (Scheme 1), with $M_{n,NMR}$ = 28.4 kg mol^{-1}, $M_{n,SEC}$ = 20.1 kg mol^{-1}, $Đ_{SEC}$ = 1.22. This use of orthogonal polymerization techniques results in the location of the DTM fluorophore between hydrophobic and hydrophilic blocks, so that subsequent self-assembly by direct dissolution in water, produces block copolymer micelles with the DTM fluorophore at the core–corona interface. DLS analysis indicated micelles with a diameter of approximately 50 nm (Fig. S4† and Tables 1, S2†). Zeta potential was measured as −27 mV, showing that the micelles also had a slightly negative surface charge (Fig. S3†). The morphology of the spherical micelles[31] was confirmed by TEM (using a graphene oxide substrate), where the size of the particles was consistent with observation of the micelle core (Fig. 1B).

Nanoparticles are well tolerated and efficiently internalized by postnatal SVZ neural stem cells

Following birth, neurogenesis takes place mainly in restricted neurogenic areas, such as the SVZ, from a highly specialized cell population known as NSC, which can give rise to neurons, astrocytes and oligodendrocytes, thus contributing the adult brain homeostasis.[3] These characteristics have triggered interest in these cells as strong candidates for stem-cell based brain repair strategies.[4] Previous studies suggest that PEI- and PLGA-based nanoparticles can be internalized into SVZ NSC and deliver active pharmaceutical molecules aiming at controlling the neuronal differentiation potential of these cells toward inducing neurogenesis in the adult brain.[4,15] Here, we developed an approach to directly image internalization of polymeric nanoparticles by means of fluorescent tagged molecules, and as a second step assess their potential as drug delivery systems. The cellular uptake and internalization potential of two different types of fluorescent nanoparticles, organic *N*-isopropylacrylamide (RM1) based nanogels and DTM-labelled block copolymer micelles (RM2) was evaluated. Adherent monolayers of NSC isolated from the postnatal SVZ by means of MACS sorting for CD 133^+ followed by enrichment through neurosphere culture were used.[32] Cells were exposed to different concentrations of RM1 and RM2 fluorescent nanoparticles for different time periods, and their intracellular internalization was studied by fluorescence microscopy.[32]

Fluorescently labelled RM1 and RM2 nanoparticles (from 40 to 150 μg ml^{-1} concentration) were applied to adherent NSC cultures and their uptake monitored at regular intervals, from 4 up to 48 h (see Fig. S5† for data at 48 h). The nanoparticles were well tolerated by the NSC, as assessed by morphological evaluation, although mild flattening of the processes was observed in the cultures treated with RM2 (Fig. 2a–f) and they could be identified within the cytoplasm of the cells (additional images in Fig. S6†). In the case of PLGA nanoparticles, with an average particle size of 200 nm, the internalization was observed 3 h post treatment while for the majority of the other nanoparticles 24 hours were required to observe internalization.[15] The minimum time for the internalization of nanoparticles in NSC is reported to be one hour for PEI based nanoparticles with a size of 224 nm. Nanoparticles can still be identified mainly in the cytoplasm of the NSC after 18–24 hours.[4] We observed internalization of both RM1 and RM2 nanoparticles (at a minimal concentration of 70 μg ml^{-1}) after 4 hours. The nanoparticles were identified in the cytoplasm of NSC with a punctate distribution, while the nucleus was spared, an observation which is in line with previous reports.[19] The fluorescence of the nanoparticles was not quantified in these experiments, as the confocal microscopy only provides qualitative measurements. The purpose of these studies carried out using fluorescent nanoparticles was to confirm internalisation and therefore validate the data obtained from the MTT proliferation assay.

Next, we set up to assess whether essential biological functions of NSC were altered by the nanoparticles. Viability/proliferation was assessed at two different time points (4 and 24 hours) post treatment with different concentrations of RM1 and RM2 (40, 70 and 150 μm ml^{-1}) (Fig. 2g and h). Cell viability/proliferation, as assessed by the MTT assay, was not significantly affected at 4 hours by any concentration of nanoparticles (mean viability ≥95% as compared to 100% viability in the control sample where no nanoparticles were added, Fig. 2g). Only a mild but significant reduction of viability was noted for RM2 (≥90% as compared to untreated cells, Fig. 2h) 24 hours after treatment. In general, NIPAM based nanoparticles (RM1) were better tolerated in comparison with RM2, regardless of the concentration. However, viability was high (at above 90%) for both NPs.

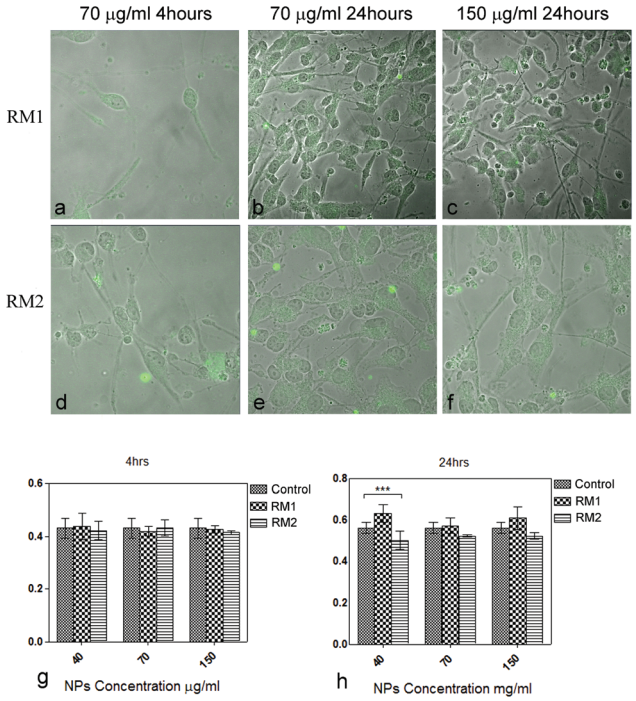

Fig. 2 Internalization of nanoparticles from SVZ NSC. Confocal microscopy microphotographs of cells treated with RM1 and RM2 at 4 h and 48 h and concentration of 70 and 150 μg ml^{-1} (a–f). MTT Proliferation Assay of the cells treated with different concentration of RM1 and RM2 nanoparticle, graphs g and h, (time of incubation with nanoparticles was 4 hours). MTT assay was performed at t = 4 h and t = 24 h.

Nanoparticles do not impair multipotency and self-renewal of murine neural stem cells

Next, the impact of the nanoparticles on the multipotency and self-renewal of NSC was analysed. NSC are capable of trilineage differentiating into neurons, astrocytes and oligodentrocytes.[33,34] To assess the impact of the nanoparticles on the multipotency of NSC, their ability to differentiate was tested. Adherent monolayers of NSC were treated with either RM1 or

RM2 at a concentration of 70 μg ml^{-1} and induced to differentiate by switching them into a neurobasal medium with B27 supplement but without growth factors, epidermal (EGF) and basic fibroblast (FGF), which would otherwise prevent their spontaneous differentiation. Quantification of the number of astrocytes, neurons and oligodendrocytes arising from treated and control cultures show no significant impact of the NPs treatment on their differentiation capability (Fig. 3).

To assess the self-renewal capacity of NSC treated with the nanoparticles, adherent monolayers, which had been treated with 70 μg ml^{-1} of either RM1 or RM2, were allowed to grow to confluency and then replated in neurosphere inducing conditions.[32] The formation of neurospheres was recorded and the cultures dissociated and replated three times (Fig. 4). Neurospheres were obtained in all cultures and no significant impact on the efficiency of neurosphere formation was observed (Fig. 4).

Taken together these experiments demonstrate that NCSs treated with RM1 or RM2 at a concentration up to 70 μg ml^{-1} retain their cardinal features of multipotency and self-renewal

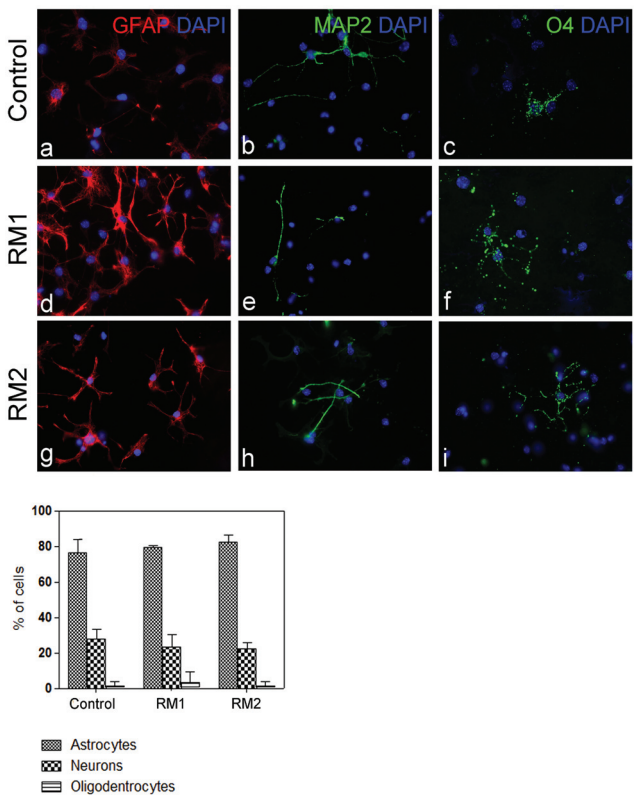

Fig. 3 Assessment of multipotency of SVZ NSC before (control) and after exposure to RM1 and RM2 nanoparticles (concentration: 70 μg ml^{-1}). Representative pictures showing the typical morphology of GFAP-positive astrocytes (red) (a, d, g), MAP2-positive neurons (green) (b, e, h), O4-positive oligodentrocytes (green) (c, f, i) and DAPI staining (blue nuclei) in the untreated cells (control) (a–c) and in cells treated with RM1 (d–f) or RM2 (g–i) nanoparticles (concentration: 70 μg ml^{-1}). The percentage of neurons, astrocytes and oligodendrocytes after 5 days of differentiation in control and cultures treated with RM1 and RM2 (concentration: 70 μg ml^{-1}) is shown in the graph.

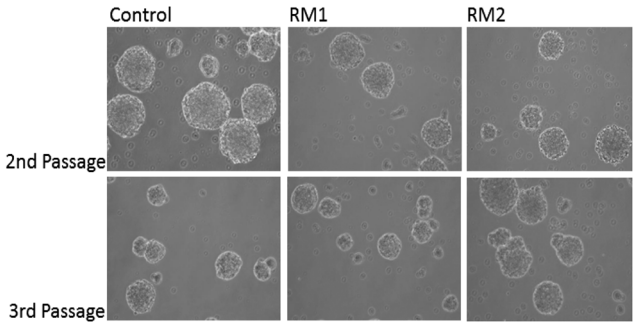

Fig. 4 Assessment of self-renewal. Neurospheres originating from SVZ NSC treated with nanoparticles (RM1 and RM2, concentration: 70 μg ml^{-1}) or untreated (control) for 4 hours. The neurospheres were dissociated and replated three times.

and raise the possibility that they could be used as a drug delivery vehicle to NSC. Interestingly the data suggest that the differences in chemical structure, with RM1 being a covalently cross-linked system and RM2 a self-assembled micelle matrix, do not significantly impact their potential as drug delivery systems for NSC. This may suggest that size, which is in fact comparable between the two systems, is playing a major role in determining toxicity and cellular uptake.

Retinoic acid (RA) uploading on nanoparticles and pharmacological effect on NSC

Many pharmaceutical agents face the challenge of decreased bioavailability as a result of poor aqueous solubility and short half-life. Moreover the administration route or frequency can often cause undesired side effects. Encapsulation of the bioactive factor in a polymer matrix can significantly increase solubility and bioavailability and therefore enhance pharmacological activity. For the purpose of this study retinoic acid was chosen as the model drug based on its two main characteristics. It is a pharmaceutically active molecule that faces the challenge of being practically insoluble in aqueous solutions and it is also known to play an important role in controlling neuronal differentiation of NSC.[35] It is important to highlight that given the extremely low solubility in aqueous phase, this drug when tested *in vitro* needs to be partially solubilized by the addition of small percentages of DMSO (0.6% in culture media). Furthermore the drug alone cannot reach the blood brain barrier and therefore requires an excipient to solubilize and favor permeation.

For the uploading of retinoic acid on the thermoresponsive nanoparticle, RM1, a modified version of a previously published protocol was utilized.[36] Retinoic acid was diluted in an appropriate solvent containing the dispersed nanogels. In an effort to maximize the uploading, the experiment was conducted at 4 °C. At this temperature the cross-linked network of nanogel is swollen, allowing the dissolved molecules of the drug to be incorporated with the possible creation of hydrogen bonds. The RM1 nanoparticles and retinoic acid solution were stirred for 72 hours to promote formation of a complex

Table 2 Polymer chemical yield, drug loading (wt%) and entrapment efficiency (wt%) of retinoic acid-loaded nanoparticles

Sample	Yield, %	Drug loading, %	Entrapment efficiency, %
RM1	72	4.72	35.9
RM2	84	0.11	9.2

between the carboxylic acid of retinoic acid and secondary amine groups of the fluorescent tag available on the polymeric cross-linked network. The nanogels were then isolated by dialysis and freeze dried. The yield as well as drug loading and entrapment efficiency for sample RM1 were determined by UV-Vis spectroscopy (Table 2), using the calibration curve (Fig. S7†).

Unlike the cross-linked nanogels, the spherical micelles were not stable to organic solvent; therefore particles were loaded *via* self-assembly in the presence of retinoic acid. Polymer and retinoic acid were mixed in a solution of dichloromethane, before removal of the solvent. Addition of water achieved self-assembly by direct dissolution, with dialysis to remove non-encapsulated retinoic acid. A portion of the resultant micelle solution was freeze-dried, allowing yield, drug loading and entrapment efficiency to be determined by UV-Vis spectroscopy.

Comparison of data obtained for the two sets of nanoparticles demonstrated that in the case of RM2 both drug loading and entrapment efficiency were considerably lower than for NIPAM-based nanogels (RM1). Attempts to increase encapsulation efficiency for RM2 by using a 100× higher quantity of retinoic acid were unsuccessful, with only 0.11% drug loading obtained. It has been previously reported that polymeric micelles with an unmodified polyester core have low entrapment efficiencies,[37] leading to the decision of evaluating the pharmacological activity using only RM1 nanogels.

The NIPAM based nanogels were also chosen because of their thermoresponsive characteristics, which allows them to undergo conformational changes as a function of temperature. This property is dependent on the chemical structure of the nanogel and the degree of crosslinking. The thermoresponsive characteristics of RM1 were studied using UV-vis spectroscopy and monitoring the change of transmittance as a function of temperature in both water and medium. The data (Fig. S8†) show that RM1 nanogels respond around 37 °C in water, and around 38.5 °C in medium. This ensured that the drug would be released when the loaded nanogels were incubated with the cells.

In order to evaluate the pharmacological effect to the NSC, retinoic acid loaded nanogels (RM1 + Ret), at a concentration of 70 μg ml^{-1}, were incubated for 48 hours with neural stem cells in medium not containing growth factors at 37 °C. After this time the nanoparticles were removed, new fresh medium, without growth factors, was added and the cells were allowed to differentiate for 5 days. We already demonstrated that at 70 μg ml^{-1}, nanogels do not affect the main characteristics of viability, multipotency and self-renewal of the NSC. Based on the entrapment efficiency calculated for RM1, the maximum concentration of the RA delivered to the SVZ NSC would be 4.6 nM. In order to evaluate the pharmacological effect of the cargo release, a solution of RA of similar concentration was also added. However given the almost complete insolubility of RA in water, 0.6% of DMSO had to be added. As previously reported, most *in vitro* studies using cultures of NSC isolated from the SVZ and hippocampus, suggest that RA exposure stimulates neurogenesis and neuronal maturation.[38]

Fig. 5 shows the results which clearly indicate that there is a significant increase in the percentage of neurons formed in both samples, the one treated with the loaded nanogels (RM1 + Ret) as well as the positive control (+Ret). Given that it was previously demonstrated that RM1 nanogels had no impact on differentiation, this result can only be attributed to the release of retinoic acid. The observation that the RA-loaded RM1 particles provide very similar results to the positive control demonstrates the potential efficiency of the delivery system. Our results are in good correlation with previous reports where

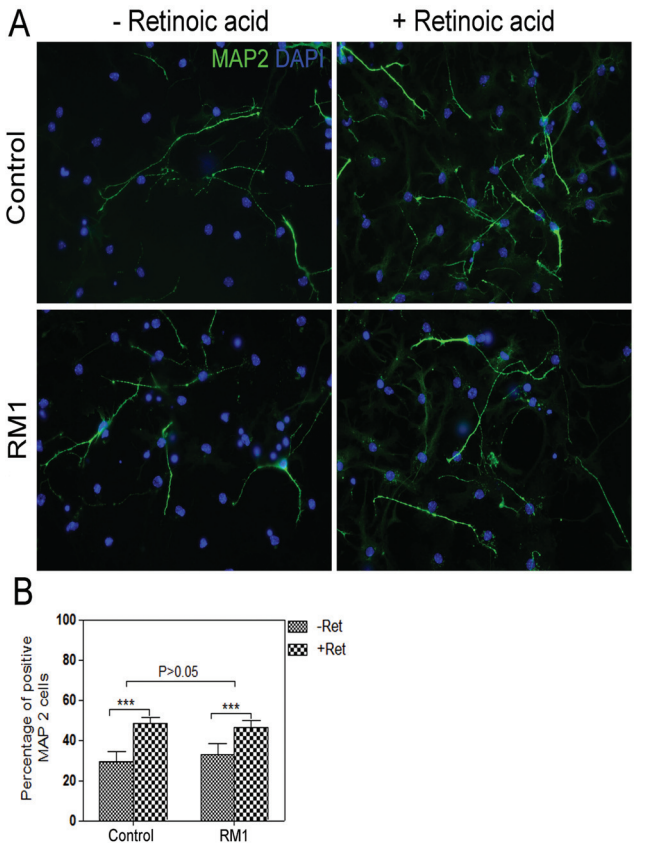

Fig. 5 Impact of retinoic acid release from RM1 on SVZ NSC differentiation. (A) Representative pictures showing a typical morphology of MAP2-positive neurons (green) and DAPI staining (blue nuclei) in differentiated NSC cultures in the absence (negative control) or in the presence of RA (positive control) and RM1 loaded nanoparticles (70 μg ml^{-1}, 4.6 nM in RA). (B) Percentage of neurons after 5 days of differentiation in control cultures and in cultures exposed for 48 hours to a concentration of 70 μg ml^{-1} RA. Retinoic acid (4 nM) solutions were prepared using 0.6% DMSO to solubilise the drug.

the formation of neurons can be enhanced with concentrations of retinoic acid between 4 and 40 nM.[4] Given the drawbacks of retinoic acid as NSC drug *e.g.* its extremely low water solubility, the formulation of this drug into nanoparticles may be an alternative approach for delivering such hydrophobic drug in the brain. NIPAM based nanogels are uptaken by the NSC, where they remain in the cytoplasm for at least 24 hours as demonstrated by the data. This time length is sufficient for the nanogels to react in terms of thermoresponsiveness to the temperature of the environment. At 37 °C, the nanogels shrink allowing the loaded retinoic acid to be released by diffusion and give rise to the pharmacological effect of the enhanced formation of neurons.

Conclusion

In this study we demonstrate that NIPAM nanogels and P(TEGA)-*b*-P($_{D,L}$LA)$_2$ based micelles are taken up and internalized in the cytoplasm of the SVZ neural stem cells, without having any significant impact on their proliferation, differentiation and self-renewal properties. The fluorescent labeling of the nanoparticles *via* covalent bonds ensures that *in vitro* tracking, for the purpose of demonstrating internalization, is accurate and removes uncertainty due to leaking. Interestingly the variation in chemical structure between the two systems does not appear to impact toxicity and cellular internalization, suggesting that size, instead, is a key feature in this regard. However the structural features do play a significant role in determining the loading capacity and entrapment efficiency and in fact RM2, the micelle system, shows a significantly lower loading capacity, as a result of the compact packing of the amorphous poly(D,L-lactide) core, and was therefore not used further. The thermoresponsive nanogels RM1 can be used in concentrations up to 150 μg ml^{-1}, significantly higher than previously reported[17] and were synthesized to respond to temperatures around 37 °C. When loaded with retinoic acid the nanogels can be easily dissolved in aqueous solutions and show a clear pharmacological effect, with increase in neurons production, as a result of modulation of SVZ neural stem cells. The high concentration of nanogels that can be used, together with the good loading efficiency and the thermoresponsive properties, ensures higher bioavailability for small drug molecules, such as retinoic acid that is practically insoluble in water, as well as tailored delivery around 37 °C. These data are promising for a future application of these nanoparticles for drug delivery.

Materials and methods

Materials

All-trans retinoic acid, *N*-isopropylacrylamide, *N*,*N*′-methylenebisacrylamide, azobisisobutyronitrile (AIBN), were purchased from Sigma-Aldrich. Dimethyl sulfoxide (DMSO) and dichloromethane were acquired from Fisher. The dual functional initiator,[39] thiourea catalyst,[40] and TEGA,[41] were synthesized as previously reported. D,L-Lactide was donated by Purac and further purified/dried over 4 Å molecular sieves in dichloromethane before being dried under vacuum and sublimed. (−)-Sparteine was dried over CaH_2 and distilled prior to use. All other reagents were used without further purification.

Synthesis of fluorescent nanogels (RM1)

Nanogels were prepared by high dilution radical polymerization as previously described.[28] *N*-Isopropylacrylamide, *N*-2-(6-(4-methylpiperazin-1-yl)-1,3-dioxo-1*H*-benzo[*de*]isoquinolin-2(3*H*)-yl-ethyl)acrylamide, *N*,*N*′-methylenebisacrylamide, in molar ratios of 75 : 5 : 20 respectively, were dissolved in anhydrous DMSO with 1% AIBN and reacted at 70 °C for two days. The clear solution was dialyzed against water for 2 days with frequent changes. Nanogel solution was frozen and lyophilized to give a white dry powder, which was stored at room temperature.

Polymer synthesis and preparation of polymeric nanoparticles (RM2)

The fluorescent poly(TEGA)-poly(D,L-lactide) amphiphilic block copolymer was prepared as described previously.[28]

Poly(D,L-lactide)

To a solution of dual functional initiator (70.0 mg, 0.11 mmol), D,L-lactide (0.641 g, 4.4 mmol), and thiourea catalyst (82.3 mg, 0.22 mmol) dissolved in dry DCM (6.41 mL) was added (−)-sparteine (25.5 μL, 0.11 mmol). The reaction was stirred at room temperature for 2 hours to a monomer conversion of 100%, before precipitation into an excess of *n*-hexane. The solid was filtered off and then redissolved in a good solvent and re precipitated again into an excess of hexane. The resultant polymer was purified *via* a prep SEC column, to yield a yellow solid. $M_{n,NMR}$ = 6.7 kg mol^{-1}, $M_{n,SEC}$ = 9.8 kg mol^{-1}, $Đ_{SEC}$ = 1.08. Size exclusion chromatography (SEC) measurements were conducted using a Varian 390-LC-Multi detector suite fitted with differential refractive index (DRI), and UV-Vis or photodiode array (PDA) detectors. A guard column (Varian Polymer Laboratories PLGel 5 μm, 50 × 7.5 mm) and two mixed D columns (Varian Polymer Laboratories PLGel 5 μm, 300 × 7.5 mm, MW cut-off ~400 000 g mol^{-1}) were used with a 500 μl sample loop. The mobile phase was tetrahydrofuran with 2% triethylamine at a flow rate of 5.0 ml min^{-1}.

Amphiphilic block copolymer

A solution of poly(D,L-lactide) (25 mg, 3.71 μmol), TEGA (80.0 μL, 0.408 mmol), and AIBN (0.152 mg, 0.926 μmol) in $CHCl_3$ (240 μL) was added to a polymerization ampoule. The solution was degassed by three freeze–pump–thaw cycles and sealed under N_2. The reaction was stirred at 60 °C for 16 hours to a monomer conversion of 95%, at which point the reaction was quenched by rapid cooling with ice bath. The solvent was removed *in vacuo*, and the residue was purified by dialysis (MWCO 6–8000 Da) against distilled water. The product was obtained as a fluorescent yellow waxy solid by lyophilisation

from water ($M_{n,NMR}$ = 28.4 kg mol^{-1}, $M_{n,SEC}$ = 20.1 kg mol^{-1}, $Đ_{SEC}$ = 1.22). Self-assembly was achieved by direct dissolution; the amphiphilic block copolymer (10.4 mg) was dissolved in water (18.2 MΩ cm) at 1 g L^{-1}, and sonicated for 3 h to afford solutions of polymeric micelles.

Characterization of nanoparticles

The morphology of the nanoparticles was evaluated by transmission electron microscopy (JEOL 2000FX). For both systems a drop of nanoparticle solution (10 μL, 1 g L^{-1}) was placed on a graphene oxide support film on Lacey carbon on 400 mesh Cu grid (Agar Scientific). After 1 minute the excess solution was wicked away, and the TEM grid was placed in a desiccator for 30 min before imaging.

Particle sizes and zeta potentials were determined using light scattering *via* Malvern Zeta-Sizer, with solutions filtered before analysis. Micelles (RM2) were analyzed directly after self-assembly, while nanogels (RM1) were suspended in water (0.1 mg ml^{-1}) and sonicated for a short time (1 min). Size Measurements were performed at 25 °C. All measurements were performed in triplicates and the results were reported in terms of mean diameter ± SD.

Preparation of retinoic acid loaded nanoparticles

Encapsulation of retinoic acid in the NIPAM nanogels (RM1) was achieved as described below. Retinoic acid was diluted in acetonitrile (ACN) under N_2 atmosphere (stock solution 1 mg ml^{-1}). 10 mg of freeze-dried nanogels were dispersed in 4 ml of ACN at room temperature. 1 ml of stock solution of diluted retinoic acid was added (ACN) to the polymer solution and incubated at 4 °C for 72 hours with stirring. The samples were then centrifuged at 20 °C, 5000 rpm for 20 min. The nanoparticles were washed trice with ACN to remove any remaining drug. The combined organic phases, containing the un-encapsulated drug, were analysed by UV-vis spectroscopy by monitoring absorbance at 364 nm and using the extinction coefficient ε_{364} = 60 200 M^{-1} cm^{-1} previously determined from the calibration curve. The loading was therefore determined by difference between the amount of drug added to the solution and the drug that remained unloaded. The nanogels obtained after centrifugation were stored under vacuum at 4 °C until further experimental use. All samples were analyzed in triplicate. Nanoparticle yield, drug loading and drug entrapment efficiency were calculated based on previously described equations.[42]

Encapsulation of retinoic acid, into the polymer micelles (RM2) was achieved as described below. Retinoic acid was dissolved in dichloromethane to give a stock solution of 0.15 mM. Polymer (9.7 mg), retinoic acid stock solution (0.65 ml) and dichloromethane (9.05 ml) were mixed to give a final polymer concentration of 1 g L^{-1} and final retinoic acid concentration of 15 μM. Dichloromethane was removed *in vacuo*, before addition of water (18.2 MΩ cm) and sonication to effect micelle self-assembly *via* direct dissolution. Excess retinoic acid was removed by dialysis against water (18.2 MΩ cm). To determine the yield, drug loading and entrapment efficiency 1 ml of the micelle solution was freeze-dried and redissolved in dichloromethane. A UV-vis spectrum was recorded, and compared with individual spectra of the polymer (Fig. S5†), and with a retinoic acid calibration curve. From these spectra the drug loading could be calculated, using the measured extinction coefficients of retinoic acid (ε_{364} = 60 200 M^{-1} cm^{-1}) and RM2 (ε_{305} = 18 400 M^{-1} cm^{-1}).

SVZ NSC cultures and experimental treatments

Mice were culled at postnatal day 7 following procedures approved by the Home Office UK (Animals Scientific Procedures Act 1986, PPL 70/7275). A narrow piece of tissue containing the SVZ located in the lateral wall of the lateral ventricles was isolated from the forebrain (approximately 1–2 mm wide and 2–4 mm long). The tissue was sliced using a tissue chopper and homogenized, followed by mechanical dissociation into single cell suspension. Cells were diluted 1 : 1 in trypan blue (Fluka) to assess cell viability and counted in a Neubauer chamber. The cells were MACS-sorted for CD133 (prominin1) according to the manufacturer's protocol (Miltenyi Biotech) and the eluted CD133$^+$ cells counted with a Neubauer chamber and plated in pre-heated stem cell culture media in ultra low attachment 6-well plates (Corning) with a concentration of 10 000–20 000 cells per cm^2 in 2 ml stem cell culture medium per well. The culture media was composed of DMEM-F12 (GIBCO) supplemented with basic fibroblast growth factor, 20 ng ml^{-1} (bFGF) (Peprotech), epidermal growth factor, 20 ng ml^{-1} (EGF) (Peprotech) and 1% B27 (Invitrogen). Adherent monolayers of NSC were cultured in multi well plates or flasks, which had been coated with Matrigel (BD Bioscience).

Internalization studies

To assess the cellular uptake of nanoparticles by NSCs, different concentrations (0.01–500 μg ml^{-1}) of fluorescent nanogels and polymeric nano-assemblies were incubated with the cells. For the internalization studies, NSCs were seeded in 24-well plates at a density of 25 000 cells per well in 500 μl cell culture medium. 24–48 hours after plating, different amounts of fluorescent nanogels or self-assembled polymeric nanoparticles were added to the wells. Cells were incubated with nanoparticles up to 4 h at 37 °C 5% CO_2, then the medium was removed and fresh medium was added. Cells were incubated for 0, 24 and 48 h, then washed with PBS and fixed with 4% paraformaldehyde (PFA) for 10 minutes at room temperature. After further washing, plates were mounted using Vectashield mounting medium (VECTOR). Fluorescent images were acquired using an inverted confocal microscope (Zeiss 510, Inverted Meta Confocal).

MTT assay

NSC cultures were seeded in 24-well plates at a density of 25 000 cells per well in 500 μl cell culture medium as aforementioned. At least 24 hours after plating, different amounts of nanogels or self-assembled polymeric nanoparticles were added to the wells. Cells were incubated with nano-matrices

for 4 hours at 37 °C 5% CO_2. The MTT assay was performed at 4 hours and at 24 hours. Media was removed from the wells and the cells washed with PBS. MTT solution (stock solution: 5 mg ml^{-1} in PBS pH 7.4) was added into each well in a ratio 1 : 10 (MTT stock solution: medium) and plates were incubated at 37 °C for 24 h. The medium was removed, 300 μl isopropanol was added in each well and agitated thoroughly to dissolve the formazan crystals. The solution was transferred to 96-well plates and immediately read by a microplate reader at 570 nm wavelength. The experiments were performed in triplicates.

Multipotency assay

For multipotency assessment, NSCs were allowed to differentiate for 5 days *in vitro* on matrigel coated glass cover slips. Cells were seeded in 24-well plates at a density of 80 000 cells per well in 500 μl cell culture medium and allowed to attach for at least 24–48 hours. Almost confluent adherent monolayers of NSC were treated with loaded or un-loaded nanomatrices dispersed in differentiating media, for at least 4 hours (minimum time period for internalization) and up to 48 hours. The medium was then removed, fresh media was added and cells were allowed to differentiate for 5 days *in vitro*. The differentiating media was composed of serum free neurobasal media (GIBCO) supplemented with 1% of B27. After five days of incubation the cover slips were washed with PBS, fixed with 4% PFA, rewashed with PBS and processed for immunocytochemistry. At least three biological replicas were used for the experiments.

Neurosphere assay

For the self-renewal assay, NSC were seeded in 24-well plates at a density of 25 000 cells per well in 500 μl cell culture medium as aforementioned. At least 24–48 hours after plating, fluorescent nanogels or self-assembled polymeric nanoparticles were added to the wells. Cells were incubated with nanomatrices for 4 h at 37 °C 5% CO_2. After four hours the excess of nano-matrices was removed and fresh media was added. Cells were incubated until almost confluent and passaged to uncoated plates, allowed to form neurospheres. The neurospheres were dissociated and replated three times.

Immunocytochemistry

To detect intracellular antigens, cells were treated with 0.1% Triton X-100 solution in PBS for 10 min at RT. Primary antibodies were diluted in 10% normal goat serum (NGS) in order to avoid unspecific binding. Cells were incubated overnight at 4 °C in the primary antibody solution. The following day they were washed with PBS, and incubated for 45 min in the dark at RT with the corresponding secondary antibody also diluted in 10% NGS. Antibodies were used as listed below. Primary antibodies: rabbit polyclonal anti-GFAP (1 : 400) (DAKO); mouse monoclonal anti-MAP2 (1 : 400) (Sigma); mouse monoclonal anti-O4 (1 : 400) (Millipore). Secondary antibodies: Alexa Fluor 546 mouse anti-rabbit (1 : 1000); Alexa Fluor 488 anti-mouse (1 : 1000) (Invitrogen). Slides were washed three times in PBS for 5 minutes and mounted with DAPI mounting media (VECTOR). Fluorescent images, five for each sample, magnification 40×, were acquired using an epifluorescent Leica microscope.

Statistical analysis

Data are expressed as means ± standard deviation or ±standard error of mean (SEM). Statistical significance was determined by one way Anova. In case of MTT assay a two way Anova was performed. $P < 0.05$ was considered to represent statistical significance.

Author contributions

The manuscript was written through contributions of all authors. All authors have given approval to the final version of the manuscript.

Acknowledgements

This work was supported by the European Commission *via* FP7 Marie Curie Actions Fellowship to SP (grant agreement 329207), the EPSRC *via* the QMUL-Warwick University Joint Initiative 2012/13 (grant no. EP/K503411/1) and Ataxia UK award to SM. The authors wish to thank Dr Graeme Cambridge for his help with the TEM images, Dr Anaïs Pitto-Barry for zeta potential measurements.

References

1 G. Orive, E. Anitua, J. L. Pedraz and D. F. Emerich, *Nat. Rev. Neurosci.*, 2009, **10**, 682–692.
2 G. Martino and S. Pluchino, *Nat. Rev. Neurosci.*, 2006, **7**, 395–406.
3 P.-M. Lledo, M. Alonso and M. S. Grubb, *Nat. Rev. Neurosci.*, 2006, **7**, 179–193.
4 J. Maia, T. Santos, S. Aday, F. Agasse, L. Cortes, J. O. Malva, L. Bernardino and L. Ferreira, *ACS Nano*, 2011, **5**, 97–106.
5 G. Yadirgi and S. Marino, *J. Pathol.*, 2009, **217**, 242–253.
6 S. Krol, R. Macrez, F. Docagne, G. Defer, S. Laurent, M. Rahman, M. J. Hajipour, P. G. Kehoe and M. Mahmoudi, *Chem. Rev.*, 2013, **113**, 1877–1903.
7 K. B. Kurakhmaeva, I. A. Djindjikhashvili, V. E. Petrov, V. U. Balabanyan, T. A. Voronina, S. S. Trofimov, J. Kreuter, S. Gelperina, D. Begley and R. N. Alyautdin, *J. Drug Targeting*, 2009, **17**, 564–574.
8 S. Wohlfart, A. S. Khalansky, C. Bernreuther, M. Michaelis, J. Cinatl Jr., M. Glatzel and J. Kreuter, *Int. J. Pharm.*, 2011, **415**, 244–251.
9 J. Li, L. Feng, L. Fan, Y. Zha, L. Guo, Q. Zhang, J. Chen, Z. Pang, Y. Wang, X. Jiang, V. C. Yang and L. Wen, *Biomaterials*, 2011, **32**, 4943–4950.

10 S. Wagner, A. Zensi, S. L. Wien, S. E. Tschickardt, W. Maier, T. Vogel, F. Worek, C. U. Pietrzik, J. Kreuter and H. von Briesen, *PLoS One*, 2012, **7**, e32568.
11 Y. Gao, Z.-Y. Wang, J. Zhang, Y. Zhang, H. Huo, T. Wang, T. Jiang and S. Wang, *Biomacromolecules*, 2014, **15**, 1010–1018.
12 J. Kreuter, *Adv. Drug Delivery Rev.*, 2014, **71**, 2–14.
13 R. Zhang, Y. Li, Bi. Hu, Z. Lu, J. Zhang and X. Zhang, *Adv. Mater.*, 2016, **28**, 6345–6352.
14 Y. Wang, M. J. Cooke, N. Sachewsky, C. M. Morshead and M. S. Shoichet, *J. Controlled Release*, 2013, **172**, 1–11.
15 S. K. Tiwari, S. Agarwal, B. Seth, A. Yadav, S. Nair, P. Bhatnagar, M. Karmakar, M. Kumari, L. K. S. Chauhan, D. K. Patel, V. Srivastava, D. Singh, S. K. Gupta, A. Tripathi, R. K. Chaturvedi and K. C. Gupta, *ACS Nano*, 2014, **8**, 76–103.
16 P. Kastner, M. Mark, N. Ghyselinck, W. Krezel, V. Dupe, J. M. Grondona and P. Chambon, *Development*, 1997, **124**, 313–326.
17 T. Santos, R. Ferreira, J. Maia, F. Agasse, S. Xapelli, L. Cortes, J. Bragança, J. O. Malva, L. Ferreira and L. Bernardino, *ACS Nano*, 2012, **6**, 10463–10474.
18 B. Ku, J.-E. Kim, B. H. Chung and B. G. Chung, *Langmuir*, 2013, **29**, 9857–9862.
19 C. W. Evans, M. Fitzgerald, T. D. Clemons, M. J. House, B. S. Padman, J. A. Shaw, M. Saunders, A. R. Harvey, B. Zdyrko, I. Luzinov, G. A. Silva, S. A. Dunlop and K. S. Iyer, *ACS Nano*, 2011, **5**, 8640–8648.
20 A. Zintchenko, A. Philipp, A. Dehshahri and E. Wagner, *Bioconjugate Chem.*, 2008, **19**, 1448–1455.
21 S. M. Moghimi, P. Symonds, J. C. Murray, A. C. Hunter, G. Debska and A. Szewczyk, *Mol. Ther.*, 2005, **11**, 990–995.
22 M. P. Robin and R. K. O'Reilly, *Polym. Int.*, 2015, **64**, 174–182.
23 X.-A. Ton, B. Tse Sum Bui, M. Resmini, P. Bonomi, I. Dika, O. Soppera and K. Haupt, *Angew. Chem., Int. Ed.*, 2013, **52**, 8317–8321.
24 M. Elsabahy and K. L. Wooley, *Chem. Soc. Rev.*, 2012, **41**, 2545–2561.
25 C. Vauthier and K. Bouchemal, *Pharm. Res.*, 2009, **26**, 1025–1058.
26 G. Pyrgiotakis, C. O. Blattmann and P. Demokritou, *Sustainable Chem. Eng.*, 2014, **2**, 1681–1690.
27 M. P. Robin, P. Wilson, A. B. Mabire, J. K. Kiviaho, J. E. Raymond, D. M. Haddleton and R. K. O'Reilly, *J. Am. Chem. Soc.*, 2013, **135**, 2875–2878.
28 M. P. Robin, A. B. Mabire, J. C. Damborsky, E. S. Thom, U. H. Winzer-Serhan, J. E. Raymond and R. K. O'Reilly, *J. Am. Chem. Soc.*, 2013, **135**, 9518–9524.
29 K. Zielinska, H. Sun, R. A. Campbell, A. Zarbakhsh and M. Resmini, *Nanoscale*, 2016, **8**, 4951–4960.
30 S. C. Maddock, P. Pasetto and M. Resmini, *Chem. Commun.*, 2004, 536–537.
31 J. P. Patterson, A. M. Sanchez, N. Petzetakis, T. P. Smart, T. H. Epps III, I. Portman, N. R. Wilson and R. K. O'Reilly, *Soft Matter*, 2012, **8**, 3322–3328.
32 G. Yadirgi, V. Leinster, S. Acquati, H. Bhagat, O. Shakhova and S. Marino, *Stem Cells*, 2011, **29**, 700–712.
33 F. Doetsch, I. Caillé, D. A. Lim, J. M. García-Verdugo and A. Alvarez-Buylla, *Cell*, 1999, **97**, 703–716.
34 W. S. Reynolds BA, *Science*, 1992, **255**, 1707–1710.
35 X.-J. Li, B.-Y. Hu, S. A. Jones, Y.-S. Zhang, T. LaVaute, Z.-W. Du and S.-C. Zhang, *Stem Cells*, 2008, **26**, 886–893.
36 S. Dhanya, D. Bahadur, G. C. Kundu and R. Srivastava, *Eur. Polym. J.*, 2013, **49**, 22–32.
37 A. L. Z. Lee, S. Venkataraman, S. B. M. Sirat, S. Gao, J. L. Hedrick and Y. Y. Yang, *Biomaterials*, 2012, **33**, 1921–1928.
38 M. Kim, A. Habiba, J. M. Doherty, J. C. Mills, R. W. Mercer and J. E. Huettner, *Dev. Biol.*, 2009, **328**, 456–471.
39 C. Ma, P. Pan, G. Shan, Y. Bao, M. Fujita and M. Maeda, *Langmuir*, 2015, **31**, 1527–1536.
40 R. C. Pratt, B. G. G. Lohmeijer, D. A. Long, P. N. P. Lundberg, A. P. Dove, H. B. Li, C. G. Wade, R. M. Waymouth and J. L. Hedrick, *Macromolecules*, 2006, **39**, 7863–7871.
41 J.-H. Ryu, R. Roy, J. Ventura and S. Thayumanavan, *Langmuir*, 2010, **26**, 7086–7092.
42 S. Papadimitriou and D. Bikiaris, *J. Controlled Release*, 2009, **138**, 177–184.